Expert Systems with Applications 42 (2015) 3048–3055

Contents lists available at ScienceDirect

Expert Systems with Applications

journal homepage: www.elsevier.com/locate/eswa

Automatic detection of abnormal mammograms in mammographic images

Chun-Chu Jen *, Shyr-Shen Yu

Department of Computer Science and Engineering, National Chung Hsing University, 250 Kuo-Kuang Rd., Taichung 402, Taiwan

ARTICLE INFO

Article history:
Available online 4 December 2014

Keywords:
Digital mammography
Preprocessing
Pectoral muscle suppression
Feature extraction
Principal component analysis

ABSTRACT

This paper proposes a detection method for abnormal mammograms in mammographic datasets based on the novel abnormality detection classifier (ADC) by extracting a few of discriminative features, first-order statistical intensities and gradients. As tumorous masses are often indistinguishable from the surrounding parenchyma, automatic mass detection on highly complex breast tissues has been a challenge. However, most tumor detection methods require extraction of a large number of textural features for further multiple computations. The study first investigates image preprocessing techniques for obtaining more accurate breast segmentation prior to mass detection, including global equalization transformation, denoising, binarization, breast orientation determination and the pectoral muscle suppression. After performing gray level quantization on the breast images segmented, the presented feature difference matrices could be created by five features extracted from a suspicious region of interest (ROI); subsequently, principal component analysis (PCA) is applied to aid the determination of feature weights. The experimental results show that applying the algorithm of ADC accompanied with the feature weight adjustments to detect abnormal mammograms has yielded prominent sensitivities of 88% and 86% on the two respective datasets. Comparing other automated mass detection systems, this study proposes a new method for fully developing a high-performance, computer-aided decision (CAD) system that can automatically detect abnormal mammograms in screening programs, especially when an entire database is tested.

1. Introduction

Breast cancer is the most common cancer in women worldwide; according to the World Health Organization, claiming the lives of hundreds of thousands of women are threatened each year. With respect to the early detection of breast cancer, mammography has been shown to be the most effective and reliable method (Davies & Dance, 1990; Lau & Bischof, 1991; Siddiqui, Anand, Mehrotr, Sarangi, & Mathur, 2005) for reducing morbidity and mortality. Developing a high-performance CAD system for the detection of breast cancer is crucial to assist radiologists and physicians. However, the presence of artifacts and pectoral muscle can disturb the detection of masses and reduce the rate of accuracy in the computer-aided analysis (CAA). To enhance the image quality of mammograms, filter or segmentation technology is usually the first image processing before application of the detection algorithm to detect suspicious lesions.

Earlier preprocessing methods for breast segmentation, which is a critical stage of breast mass analysis, were generally based on global thresholding (Davies & Dance, 1990; Lau & Bischof, 1991) or gradient analysis (Chandrasekhar & Attikiouzel, 1997; Karssemeijer, 1993). Ojala, Nappi, and Nevalainen (2001) presented an algorithm to segment the breast region from digitized mammograms, but the bright objects outside of the breast region may cause errors in this segmentation. A segmented breast generally consists of the whole breast, pectoral muscles and the nipple extraction. Therefore, the pectoral muscle regions should be removed before detecting the tumor cells so that mass detection can be performed more efficiently. Former work related to pectoral muscle suppression used the Hough transform (Kwok, Chandrasekhar, & Attikiouzel, 2001); Ferrari and Rangayyan (2004) proposed a polynomial modeling of the pectoral muscle. The contrast enhancement technique on mammogram images was used before suppression of pectoral muscle (Maitra, Nag, & Bandyopadhyay, 2011). To make the mass detection more effec-

* Corresponding author.
E-mail addresses: phd9717@cs.nchu.edu.tw (C.-C. Jen), pyu@nchu.edu.tw (S.-S. Yu).

http://dx.doi.org/10.1016/j.eswa.2014.11.061
0957-4174/

tive, an image preprocessing that applies gamma correction equalization (Gonzalez & Woods, 2008) and Otsu's thresholding method (Otsu, 1979) is presented here to segment a suitable breast region with pectoral muscle suppression.

During mass detection, masses are often embedded in and camouflaged by the varying densities of breast tissue structures; moreover, mass shapes can be spiculated, circumscribed and ill-defined. Depending on the experience of the physician, breast cancer detection can be facilitated using computerized feature extraction algorithms. Sameti, Ward, Palcic, and Morgan-Parkes (1997) divided a mammogram into different regions of mass candidates; the discrete texture features were then calculated for the area of each mass candidate. The features were computed based on gray-level co-occurrence matrices (GLCM) that requires high computational loads, and the effectiveness of the textural information possessed by mass regions in comparison with the mass margins was evaluated (Mudigonda, Rangayyan, & Desautels, 2000). Bellotti et al. (2006) characterized regions of interest (ROIs) by means of textural features computed from the GLCM. The separation of normal regions from lesions with masses could be achieved using texture features (Roberto et al., 2006). Mohd Khuzi, Besar, Wan Zaki, and Ahmad (2009) also used GLCM that was constructed at four different directions for each ROI to extract the textural features. Features in the study of Yuan, Giger, Li, and Sennett (2008) were grouped into categories of texture features based on GLCM. Mohamed and Kadah (2007) extracted a large feature set and found that 78 of those features are capable of discriminating between normal and abnormal breast tissues in mammograms with a true positive (TP) rate of 83.3%. In this study, the abnormal ROI from the gray-level quantified ROIs in a mammogram can be distinguished merely by five extracted features containing 3 of first-order statistical intensities and 2 of gradients.

Over the past few years, many texture feature extraction methods have been proposed that use the calculated GLCM, and there has been an incremental computation cost of detection for large numbers of features; however, their performance is still not very promising. Here, the PCA (Pearson, 1901) technique is used to obtain the feature weights after extraction of a few representative features from the abnormal ROI in the quantized breast object. Furthermore, a novel ADC exploiting the multiple feature weight adjustments is proposed for identifying the abnormal mammograms in a database or a specified dataset. This paper not only proposes effective image preprocessing techniques and the classifier ADC based on a few of extracted features but outperforms other mentioned methods for detecting abnormal mammograms.

The rest of this paper is organized as follows: in Section 2, we specify the abnormal dataset and the databases used; in Section 3, the techniques for image preprocessing, feature extraction and classification are presented; in Section 4, the promising results are shown and compared to other mass-detection methods; and Section 5 presents some concluding remarks.

2. Image database

For the development and evaluation of the proposed method, the data used in the experiments was taken from the MIAS database (Suckling et al., 1994) consisting of 322 mammogram images in the mediolateral oblique (MLO) view and the Digital Database for Screening Mammography (DDSM) by Heath et al. (1998). The principal characteristics of the abnormalities were bright regions with irregular shapes and indistinct or spiculated margins. The authors specified set S_1, containing 113 abnormal mammograms accurately representing calcification, spiculated masses, circumscribed masses, ill-defined masses, architectural distortion, and asymmetry from the MIAS database, which was reduced to a resolution of 200 μm by pixel and clipped/padded so that every image was 1024×1024 pixels. Set S_2 consisted of 67 abnormal and 133 normal MLO-view mammograms selected from the DDSM database which has been downsized to 50% using bicubic interpolation and transformed into 256 gray levels with a size of approximately 2500×1500 pixels.

3. Methods

The mass detector (MD) CAD system for automatic detection of abnormal mammograms mainly consists of image preprocessing, mass detection and the classifier ADC. This image preprocessing of the MD system contains global equalization transformation, image denoising, binarization, breast object extraction, breast orientation determination, and pectoral muscle suppression. An overview of the research methodology is presented in Fig. 1.

3.1. Global equalization transformation

I_{in} is the input image of the gray-level digital mammogram. To normalize the range of contrast variation among different images, all gray-level intensities of the pixels within I_{in} will be stretched to the full range of 0–255. $I_{in}(x, y)$ is the intensity value of a pixel located at coordinates (x, y) and the min_{in} and max_{in} are the minimal and maximal gray-level intensities in I_{in}, respectively. I_{in} is transformed into I_s by the following formula:

$$I_s(x,y) = 255\left(\frac{I_{in}(x,y) - min_{in}}{max_{in} - min_{in}}\right) \quad (1)$$

Consequently, the intensity range of I_s is normalized to [0, 255].

3.2. Image denoising

The noise within a mammographic image could result in imprecise object extraction. Thus, the MD uses the mean filter (Gonzalez & Woods, 2008) to eliminate short-tailed noise such as uniform and Gaussian-type noise from I_s, and a neighborhood window size of 11×11 is given. I_m is the denoised image obtained by removing the noise from I_s.

3.3. Binarization

It is necessary to first identify the breast region and remove the non-breast region and information plates to reduce subsequent processing calculations. To determine the breast object, the MD utilizes Otsu's thresholding method to find the optimal adaptive threshold t_o corresponding to the intensity of I_m, and the value of t_o is approximately 70–110; it hence specifies a soft-threshold $t_s = \alpha_s t_o$, for binarizing the I_m, where α_s is a given constant less than 1. If $I_m(x, y)$ is greater than or equal to t_s, then $I_b(x, y)$ is assigned to 1; otherwise, $I_b(x, y)$ is given a 0. As a result, a binary image I_b shown as Fig. 2(a) is obtained with a given $\alpha_s = 0.6$, which can meet the aim of more complete object extraction.

3.4. Breast object extraction

The MD excludes the dark background and calculates the area of each disjoined object from I_b; it then specifies a flat, disk-shaped structuring element with a radius of 2 pixels that will be used in the study. All probable breast objects in I_b are processed by the basic morphological operations, erosion and dilation (Serra, 1982). Consequently, the largest remaining object is obtained after α_m times erosion then dilates back α_m times: the dilated object is then extracted as the breast object and denoted by I_o as shown in Fig. 2(b). Here, α_m is a given constant of 30. Moreover, the MD

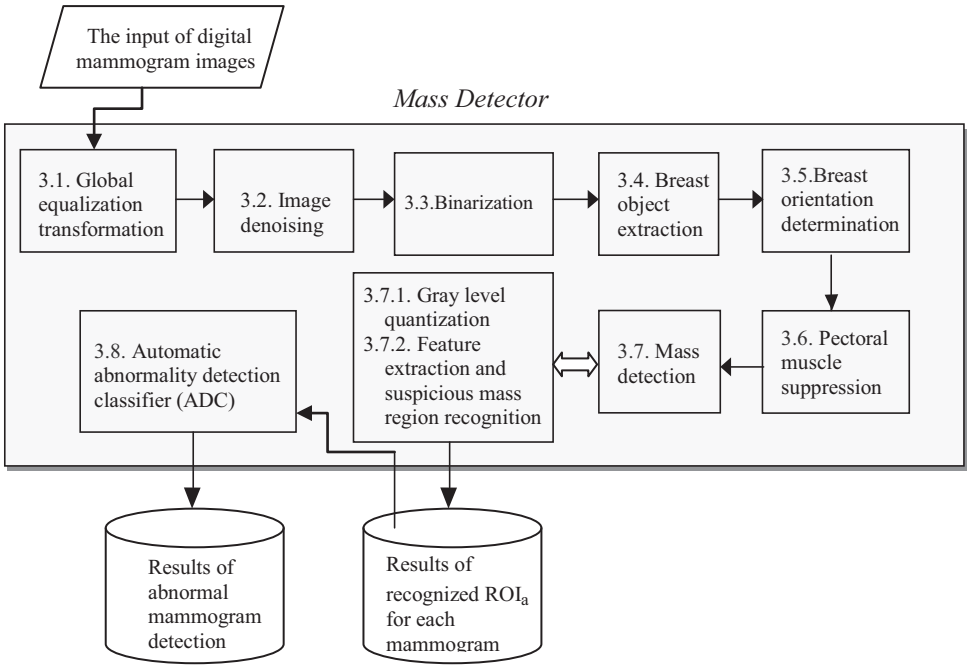

Fig. 1. The block diagram of the proposed method.

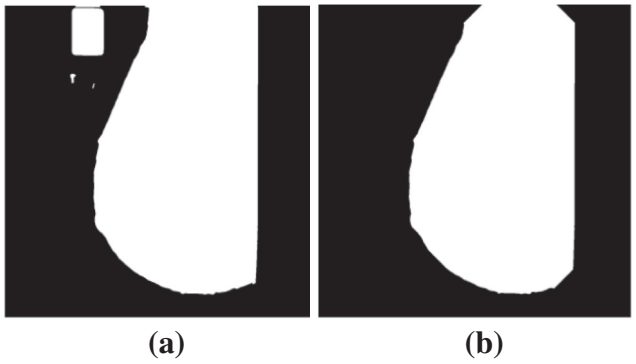

Fig. 2. (a) A binary image I_b from I_m and (b) a breast image I_o from I_b.

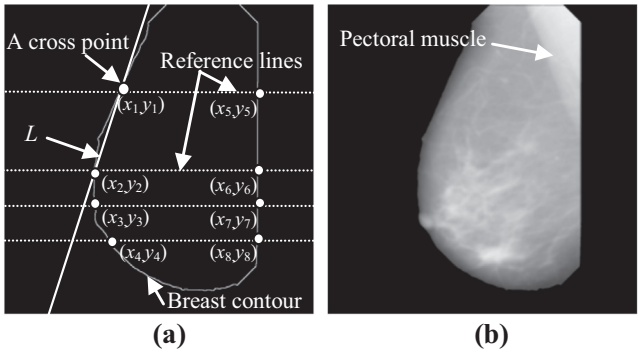

Fig. 3. (a) A breast contour I_c and (b) a breast image I_d.

calculates the gradient of I_o using Sobel operation (Gonzalez & Woods, 2008) to generate a breast contour I_c depicted by the solid border in Fig. 3(a).

3.5. Breast orientation determination

To locate the region of pectoral muscle in I_o, the MD needs to determine the orientation of I_c. At least four horizontal reference lines are assigned and spaced out 1/4 or 1/8 image height apart, depicted as dotted lines in Fig. 3(a) passing across both sides of the breast contour at eight cross points. If four cross points as indicated by coordinates (x_5, y_5), (x_6, y_6), (x_7, y_7) and (x_8, y_8) are near the pectoral muscle at the right side of Fig. 3(a), and approximate to the vertical permutation within tolerance when the inclination angle is smaller than 0.6° around 90°, then the breast orientation is specified as left of the image; vise versa for opposite side. In the case that there is no vertical permutation of cross points (i.e., there exists only an incomplete contour of I_c or lacks the vertical contour part), another judging function of the breast orientation denoted by $BO(s)$ is given as

$$BO(s) = \begin{cases} \text{right}, & s >= 0 \\ \text{left}, & s < 0 \end{cases} \quad (2)$$

where the symbol s represents the slope of the straight line L passing through two upper cross points on a non-vertical contour curve as left half of Fig. 3(a) (e.g., the slope s between two points (x_1, y_1) and (x_2, y_2) can be calculated by $s = (y_2 - y_1)/(x_2 - x_1)$; the origin is located at the top-left corner of the image). Additionally, a breast image I_d with pectoral muscle corresponding to I_m judged as left orientation is shown in Fig. 3(b).

3.6. Pectoral muscle suppression

The pectoral muscle shown on the right side of Fig. 3(b) is brighter than the rest of the breast tissue. To separate the pectoral muscle from I_d, the MD applies gamma correction equalization to enhance the contrast of I_d by computing

$$I'_\gamma(x,y) = 255\left(\frac{I_d(x,y) - min_d}{max_d - min_d}\right)^\gamma \quad (3)$$

where γ is a given constant, and min_d, max_d are the minimal and the maximal gray-level values of all the pixels in I_d, respectively. The contrast of I'_γ can be modified by altering the value of γ. A larger $\gamma > 1$ will emphasize the brighter areas of I_d, while a smaller $\gamma < 1$ will emphasize darker regions in I_d. Fig. 4(a) shows the image I'_γ obtained by formula (3) for the given $\gamma = 7.5$. To find the optimal adaptive threshold t_p, Otsu's thresholding method is used by MD and another soft-threshold $t'_s = \alpha'_s\ t_p$ is specified for binarizing I'_γ. After the binarization, the image I'_b, shown as Fig. 4(b), is obtained by a given constant $\alpha'_s = 0.7$.

One of the relatively large objects within I'_b is considered as the pectoral muscle. Hence, the MD first executes morphological operations, α'_m times erosion on I'_b and then dilates back α'_m times for reserving candidates of the pectoral muscle, and the given value of α'_m is 12. Second, MD specifies the nearest reference coordinates of the pectoral muscle (*NRCPM*) in I'_b and the *NRCPM* is defined as follows:

$$NRCPM(o) = \begin{cases} (1,1), & \text{if } o = \text{right} \\ (1,\mathrm{w}), & \text{otherwise} \end{cases} \quad (4)$$

where the symbol for argument o represents the breast orientation determined in previous Section 3.5 and w is the pixel width of I'_b. Third, MD computes the minimal Euclidean distance (Gray, 1997) between these pectoral muscle candidates and the judged *NRCPM* then removes the determined pectoral muscle from I'_b; finally, all remaining regions separated are the segmented ROIs, shown in Fig. 5(a). An image I'_d obtained by removing the pectoral muscle from I_d is shown as Fig. 5(b).

3.7. Mass detection

Each ROI shown in Fig. 5(a) is considered as a candidate of mass region for further mass detection. Based on the discriminative features extracted, the following recognition method is able to detect a suspicious mass region from all ROIs processed by gray level quantization in a mammogram.

3.7.1. Gray level quantization

The image I'_d having the range of 256 gray levels is transformed into a 32 quantization level image of I'_q (Shi & Sun, 2008) for further feature extraction. The MD subsequently extracts discriminative intensity and gradient features from each of various ROIs corresponding to the pixel intensities of I'_q.

3.7.2. Feature extraction and suspicious mass region recognition

For each ROI, the five extracted features are described as follows: the mean (μ), the standard deviation (σ) of the total pixel intensities, the number of different layer heights (n_l) in which the pixel intensities are equivalent on a layer of the same height,

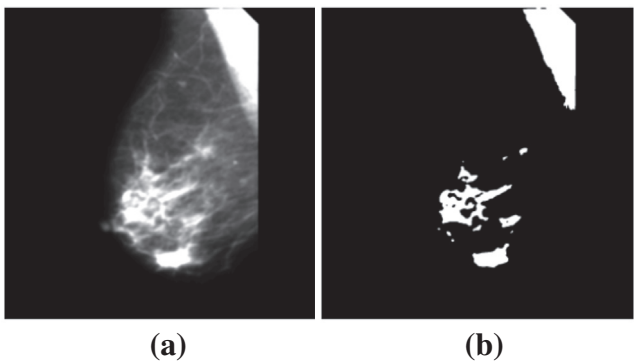

Fig. 4. (a) I'_γ obtained from I_d and (b) the image I'_b obtained from I'_γ.

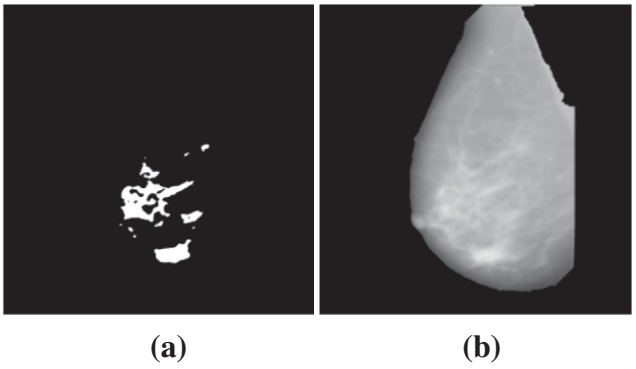

Fig. 5. (a) ROIs from I'_b. (b) I'_d with a *NRCPM*(o) of coordinates (1, 1024).

i.e., the number of different quantized levels, the mean gradient (μg) and the total gradient (sg), both of which extract only the gradient pixel values greater than 0 and less than a specified threshold $t_g = \mu_{ROIg} + \alpha_g s_{ROIg}$, where the mean gradient μ_{ROIg} and the standard deviation s_{ROIg} are obtained by applying the Sobel operation on the ROI and $\alpha g = 2.0$ is given to reduce the variation range. In statistics, the mode is the value that occurs most frequently in a dataset; hence, MD first calculates the μ, σ, n_l, μg and sg in each ROI corresponding to I'_q and then finds out the largest frequency values of μ, σ, n_l, μg and sg and records their individual ROI indices denoted by $X\mu$, $X\sigma$, X_{n_l}, X_{μ_g} and X_{s_g}. The formula $X_{ROI} = \mathrm{mode}(X\mu, X\sigma, X_{n_l}, X_{\mu_g}, X_{s_g})$ calculated by the mode function is used to identify the index of the abnormal ROI, therefore the ROI corresponding to X_{ROI} is then recognized as the suspicious mass region and denoted as ROI_a on the mammogram.

3.8. Automatic abnormality detection classifier (ADC)

This subsection develops a two-stage classifier denoted as ADC for automatic detection of abnormal mammograms based on the features μ, σ, n_l, μ_g and s_g extracted from the ROI_a. In the first stage, PCA technique is used to compute eigenvalues for the first defined abnormal and normal feature difference matrices, the initial feature weights would be obtained. After that, the ADC calculates respective centroid coordinates for the two feature difference matrices using the proposed feature weight adjustment algorithm and then generates two rows of normalization denominators for further calculation. In the second stage, by measuring two different Euclidean distances between the tested image that is adjusted by multiplying respective weight factors then divided by the normalization denominators and the corresponding centroid coordinates, the ADC can automatically detect if an abnormality exists in a tested image for the entire mammographic dataset and it can be briefly described as follows:

The automatic ADC algorithm

Step 1. In the first stage, to define a C_a of $n \times 5$ (n is the number of mammograms) real matrix of feature differences away from the means, containing n abnormal row elements of $[|\mu - \mu_{mean}|_{1,1}\ |\sigma - \sigma_{mean}|_{1,2}\ |n_l - n_{l\ mean}|_{1,3}\ |\mu_g - \mu_{g\ mean}|_{1,4}\ |s_g - s_{g\ mean}|_{1,5}]_{1\times5}$ detected correctly by MD for representing the absolute values of the differences which are μ, σ, n_l, μ_g and s_g of the ROI_a minus respective means from all ROIs in a mammogram; likewise, define a C_n containing non-zero normal images and less than the total number of normal mammograms in a database.

Step 2. Compute the standard deviation σ_i for each of corresponding column space c_i in $C_a = [c_1, c_2, c_3, c_4, c_5]$, and then standardize the different variation by $M_{s1} = [c_1/\sigma_1, c_2/\sigma_2, \ldots, c_5/\sigma_5]$, therefore, relatively larger element values in

different column spaces can be avoided then the five distinct eigenvalues $\lambda_1 \leqslant \lambda_2 \leqslant \lambda_3 \leqslant \lambda_4 \leqslant \lambda_5$ are obtained by using PCA technique; M_{s2} is obtained from C_n as M_{s1}.

Step 3. Calculate the weight factor $w_i = \frac{\lambda_i}{\sum_{j=1}^{5}\lambda_j}$ $(i = 1,2,\ldots,5)$ for corresponding c_i $(i = 1,2,\ldots,5)$ in C_a and then generate the $C_{wa} = [c_1 \times w_1, c_2 \times w_2, \ldots, c_5 \times w_5]$ to increase importance level from c_1 to c_5, which can be in accordance to the discrimination ability of the features; normalize all elements for respective weight-adjusted columns of C_{wa} to [0,1], therefore the normalized result is denoted by C_{na}; C_{wn} and C_{nn} are obtained from C_n as C_{wa} and C_{na}.

Step 4. Consider the C_{na} as a five-dimensional feature space and then calculate the centroid coordinates by $cc_{na} = \left(\frac{\sum_{k=1}^{r} e_{k1}}{r}, \frac{\sum_{k=1}^{r} e_{k2}}{r}, \ldots, \frac{\sum_{k=1}^{r} e_{k5}}{r}\right)$, where r is the number of total row elements and e_{ki} is the element lying in the kth row and ith column of C_{na}; similarly, cc_{nn} is obtained from C_{nn} as cc_{na}.

Step 5. Compute two rows of normalization denominators denoted by $M = [m_1, m_2, \ldots, m_5]$ and $N = [n_1, n_2, \ldots, n_5]$; first, to concatenate C_{wa} and C_{wn} into a cascaded $C_{an} = [z_1, z_2, z_3, z_4, z_5]$, then adjust the weights of C_{an} by multiplying the corresponding w_i of C_a, as a result, $M = [MAX_z\{z_1 \times w1\}, MAX_z\{z_2 \times w_2\}, \ldots, MAX_z\{z_5 \times w_5\}]$ is obtained that MAX_z indicates taking of the maximum element value in a weight-adjusted column elements of C_{an}; likewise, N can be obtained as M.

Step 6. In the second stage, a tested image represented as (e_1, e_2, e_3, e_4, e_5) like one of the row elements in C_a. Let d_a or d_n denote Euclidean distance for the measure, d_a is the distance from the tested image with weight-adjusted coordinates $(e'_1, e'_2, e'_3, e'_4, e'_5)$ to cc_{na}, where $e'_k = (w_k e_k)/m_k$ for $k = 1, 2, \ldots, 5$ (w_k as the weight factor w_i of C_a, m_k is a normalization denominator in M); accordingly, d_n is calculated from the cc_{nn} as d_a.

Step 7. Check the abnormality by estimating the difference of d_a^2 (square of d_a) and d_n^2 for a tested image, if $d_a^2 - d_n^2 <= 0$ then the image is considered abnormal because it is closer to C_a and farther from C_n; otherwise, the image is normal.

4. The experiments and results

In Section 4.1, three experiments were conducted to show the analytical performance of the proposed method on detecting abnormal mammograms. The MD system implemented the algorithm of ADC in Section 3.8 of this study using the MIAS for first two experiments and a dataset from DDSM in the third experiment. The authors discuss image denoising, gray level quantization, and then analyze the experimental results and make a comparison with other previously proposed mass detection methods in Section 4.2.

4.1. Experiments

In the first experiment, the MD figures out the ROI_a among all ROIs corresponding to I'_q for each image in S_1. Consequently, the MD can correctly detect 60 ROI_a. An appropriate validation is essential for the mass detection method to achieve a certain degree of precision and clinical acceptance. Sensitivity (*Sen*) determines how effective the system is in predicting a success. Here, *Sen* is used for describing the successful performance of abnormality detection and can be computed by

$$Sen = \frac{TP}{TP + FN} \tag{5}$$

where *TP* is the number of true positive images which are accurately detected as the abnormality ones by MD based on the information given by the database; *FN* is the number of false negative images that are not detected as abnormalities by MD but are indicated abnormalities from the database used.

The correct rate of abnormal mammogram detection in the first experiment is 0.53 = 60/113 and the constant $\alpha'_s = 0.7$ is given for specifying a soft-threshold t'_s to binarize I'_γ for the segmentation of ROIs. To improve the performance of MD for mass detection, the value of the adjustable parameter α'_s can be set to 0.5. As a result, the correct rate of mass detection in S_1 is increased to 0.73 = 83/113. Then, the MD implements ADC by employing the experimental result with $\alpha'_s = 0.5$; C_a contains 74 row elements selected from the correct mass detection by MD and C_n consisting of 177 row elements is selected from the normal images indicated by ground truth. Hence, the number of the training set is 251 (74 + 177) for the first stage. In the second stage, the result for all 322 test images from MIAS shows an abnormal mammogram detection with performance of *TP* = 99, *FN* = 14, *Sen* = 0.88. Fig. 6(a) and (d) show two images of abnormality detection in this experiment.

Experiment 2 is designed to discriminate the ROI_a from other segmented ROIs by adding consideration of their shapes. The MD adds geometric features containing compactness and roundness for each ROI and the mean area (μ_a) of all ROIs. The compactness (Sakai, Yonekawa, & Matsuzaki, 1996) of a region or shape is measured by the following equation:

$$C = 4\pi \frac{S}{R^2} \tag{6}$$

where *C* is compactness (dimensionless), *S* is area of the region and *R* is the perimeter of the region. The roundness (Yonekawa, Sakai, & Kitani, 1996) of a region or shape is defined as

$$R = \frac{4A}{\pi L^2} \tag{7}$$

where *R* is the roundness, *A* is the area of the region and *L* is the maximum length of a region. First, the MD eliminates the unmatched ROIs with small sizes, less than $\mu_a - \alpha_a\sigma_a$, where σ_a is the standard deviation of all ROI sizes and $\alpha_a = 1.5$ is a given constant. Second, the MD considers not only the five features in experiment 1, but also examines whether their shapes are out of the appropriate range of roundness and compactness. Based on the result analysis about 83 correctly detected images in the first experiment, the appropriate ranges are set at 0.12 < compactness < 1.19 and 0.22 < roundness < 0.92 for a ROI_a. The number of geometric features is two and less than the five of features in experiment 1, as balanced consideration the weight of the geometric feature is commonly doubled to determine the ROI_a in a mammogram. As a consequence, the correct rate of abnormal mammogram detection on S_1 is 0.76 = 86/113; the result by implementing ADC for all 322 images in MIAS shows an abnormality detection performance of *TP* = 100, *FN* = 13, *Sen* ≈ 0.89. Fig. 6(b) and (e) demonstrate two detected images in the second experiment.

In experiment 3, the ADC will work on the new dataset S_2, and the image I'_γ taking the preprocessing procedure is obtained by formula (3) for given $\gamma = 6.0$. In the first stage, C_a contains 34 abnormal images and C_n consists of 66 normal ones; they are both retrieved from S_2 for computing the reference feature components and the rest of the 100 images for validation during the second stage. The result for the 200 test images shows an abnormal mammogram detection with performance of *TP* = 57, *FN* = 9, *Sen* = 0.86. Fig. 6(c) and (f) demonstrate two detected results in experiment 3.

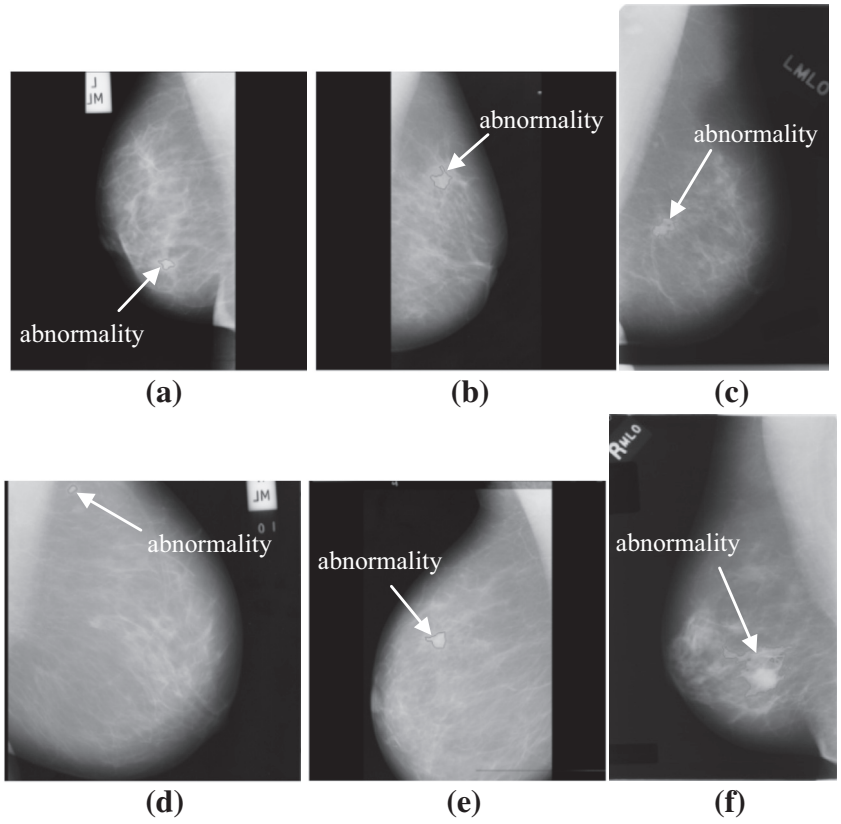

Fig. 6. (a) mdb181with the original information plate, classified as a spiculated mass (b) mdb092, classified as asymmetry (c) C_0047_1.LEFT_MLO (d) mdb144 with the original information plate (e) mdb155, classified as architectural distortion (f) C_0009_1.RIGHT_MLO, where mdbXXX is an image in MIAS database with the number of XXX and C_XXXX_1.RIGHT_MLO is the filename of an image with cancer in the DDSM database.

4.2. Discussion

In this study, we perform image denoising using a simple mean filter because screening mammography is a low-dose X-ray examination of the breast; radiographic noise occurs in random, non-random or static variation in average digital signal levels of a radiograph that has received uniform X-ray exposure (Nishikawa & Yaffe, 1985; Swank, 1973). Considering that the impact of the low pass mean filter on the small malignant tumors is not significant due to that the presence of microcalcifications is generally high density of small bright spots. For the consideration of effective feature extraction, finer quantization reducing the number of gray levels is expected to improve both accuracy and separability (Clausi, 2002). Shokr (1991) considered the effect of quantization on co-occurrence feature values and Clausi (2001) believed that using uniform quantization produced preferred results. Therefore, the authors adopted 32 quantization levels for feature extraction which can discriminate the abnormalities for an image I'_d. Moreover, other features, such as irregularity, size are considered and evaluated in the experiment 2 for examining the effect of non-homogeneity, and then the determined ROI_a is used for our ADC algorithm.

To decrease the number of false positive (*FP*) images after utilizing the ADC, we normalize all the values of d_a^2 corresponding to each of abnormal images with $d_a^2 - d_n^2 <= 0$ and initiate two separate clusters, normalized d_a^2 and the corresponding $d_a^2 - d_n^2$, for applying the K-means algorithm, then the *FP* = 34 and the number of true negative (*TN*) images = 175 could be obtained. Hence, the specificity (*Spe*) measure ($Spe = \frac{TN}{TN+FP}$) equals 0.84. To investigate more general quality for the study, the area under the receiver operating characteristic (ROC) curve (AUC) evaluated for the test set of 322 images yielded a value of 0.71 with a standard error of 0.03. Fig. 7 shows the ROC curve for the ADC with an acceptable performance (AUC 0.7–0.8). Nonetheless, the ability of generalization of ADC will be influenced by the centroid coordinates, cc_{na} and cc_{nn}, and the normalization denominators of M and N those are trained at the first stage. In other words, the performance of ADC will change when the training set contains different structure (ratio) of normal/abnormal images. Using the same testing set, the empirical results show that if the ratio of normal/abnormal images is equal to or greater than 1.5 in the training stage, the performance of ADC will be excellent and quite stable.

The authors have tested all of the 322 images in the MIAS database and a subset from the DDSM database. Table 1 shows a

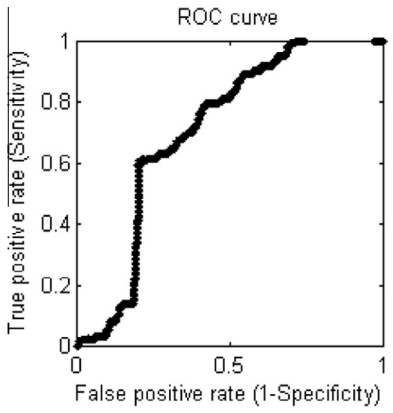

Fig. 7. ROC curve of the ADC tested for 322 images in MIAS database.

Table 1
Performance results for the different mass detection methods.

Extraction of the textural features	Authors	Digital mammogram database	The number of abnormal images used	The number of normal images used	The number of total images in the database	*Sen* (%)
GLCM	Mudigonda et al. (2000)	MIAS	26	28	322	82.1
Featureless	Campanini et al. (2004)	USF DDSM	312	200	2620	80
GLCM	Mohd Khuzi, Besar, Wan Zaki, and Ahmad (2009)	MIAS	20	20	322	72
Contrast and contour of the masses	Rojas and Nandi (2009)	43 from MIAS and 306 from DDSM	349	0	2942	62
Structural, spectral and GLCM	Martins et al. (2009)	A subset of the DDSM	433	0	2620	86
GLCM	Eddaoudi, Regrgui, Mahmoudi, and Lamouri (2011)	MIAS	76	19	322	85.5
Spatial gray level dependence (SGLD)	Meenalosini and Janet (2012)	MIAS and DDSM	125	125	2942	95.2
Intensity and gradient	Newly proposed method	MIAS	113	209	322	88
		A subset of the DDSM	67	133	2620	86

Table 2
The current literature versus the contribution of the study.

Reference	Contribution	Proposed approach	Database used
Liu, Tsai, Tsui, and Yu (2012)	Extraction of extrapolated breast object	Improved GVF snake algorithm	MIAS
Mustra and Grgic (2013)	Pectoral muscle segmentation	Adaptive histogram equalization and polynomial curvature estimation	MIAS
Agrawal, Vatsa, and Singh (2014)	Visual saliency based segmentation of probable mass regions	Saliency maps for ROI segmentation and the ROIs classification using entropy features	MIAS
Dheeba, Albert Singh, and Tamil Selvi (2014)	Design a CAD system for detection of breast abnormalities	To improve the classification accuracy using Particle Swarm Optimized Wavelet Neural Network	216 clinical mammograms collected from 54 patients
This paper	Fully develop a high-performance CAD system with presented preprocessing techniques needed for detecting abnormal mammograms	The proposed classifier ADC accompanied with the novel feature weight adjustments has the excellent ability of generalization	MIAS and a subset of the DDSM

comparative view of several mass detection methods based on individually extracted features, including the newly proposed method, by examining the number of images used in each database with a total image number and corresponding sensitivity. Even though the method described by Meenalosini and Janet (2012) has the best *Sen* = 0.95, the lower rate of images used from the two databases is 0.08 = (125 + 125)/2942 compared to ours 0.18 = (322 + 200)/2942. There is another case in Table 1 that has better performance (*Sen* = 0.86) (Martins, Junior, Silva, Paiva, & Gattass, 2009), but the case calculated textural measures using the computation-intensive GLCM technique and only tested a subset of the DDSM database. Moreover, the empirical values of used parameters such as α_s, α_m, γ, α'_s, α'_m, α_g, and α_a are determined through heuristic evaluation alone and then suitable for the effectiveness. For avoiding that a minor change of only one parameter could maybe lead to a collapse of the overall method. The 95% confidence intervals on each mean of the above parameters are presented as [0.25, 0.87], [26, 37], [6.65, 7.81], [0.45, 0.73], [5, 27], [1.45, 2.67], and [1.21, 2.18], respectively. Meanwhile, Table 2 detailed the current literature versus the contribution of the study is related to the abilities of mass detection.

5. Conclusions

This study has proposed a high-performance CAD system for detecting abnormal mammograms by using the two-stage classifier ADC, which applied the PCA-based technique accompanied by robust feature weight adjustments. To advance the difficult detection of abnormal mammograms, first we present preprocessing techniques which are needed for the detection effectiveness of breast cancer such as binarization, breast object extraction, breast orientation determination, and pectoral muscle removal. After the preprocessing steps, the MD quantizes all ROIs in a mammogram and then extracts a small number of critical features mainly consisted of first order statistical intensities and two types of gradients yielded by the suspicious ROI, which is recognized by using the mode function in subsection 3.7.2. In brief, the presented detection method merely requires five discriminative features extracted from the ROI_a by the CAD system. Hence, the challenge system can be effectively employed to detect if an abnormality exists in a digital mammogram.

According to the experiments carried out in the whole MIAS database, the ADC showed a significant impact on improving generalized classifier for mass detection with a high sensitivity of 88% and a sensitivity of 89% while additionally considering geometric features, and also obtained a specificity of 84% after our process of false positive reduction; a sensitivity of 86% was obtained for a subset from the DDSM database. The empirical performance of this proposed CAD system is promising and stable for abnormal mammogram detection compared to other previously proposed mass detection methods.

As with all research methods, there are unavoidable cases or limitations in our study. One of the limitations in this research is useless for the global equalization transformation on an extremely low-contrast mammogram due to image blurring then the breast region could not be accurately extracted. In Section 3.6 of proposed pectoral muscle suppression, while the brightness values of small

malignant tumors as microcalcifications are less than t'_s, the tumors will be lost in the binary image I'_b and the incomplete segmentation result of ROIs is caused by another limitation of brightness. The third limitation is that the ratio of normal/abnormal images should not be less than 1.5 in the training stage of ADC; otherwise the performance of abnormality detection will be significantly influenced.

In our future research, we would like to investigate other algorithm for the false positive reduction followed by the execution of ADC. We would also like to evaluate the proposed approach on other clinical databases for the consistency of abnormality detection. An optimal CAD system of detection mammograms that can dynamically adjust parameters used by this study will also be an interesting work in our future research.

Acknowledgments

The authors would like to thank the editor and reviewers for their insightful comments which have greatly helped us to improve this article.

References

Agrawal, P., Vatsa, M., & Singh, R. (2014). Saliency based mass detection from screening mammograms. *Signal Processing, 99*, 29–47.

Bellotti, R., De Carlo, F., Gargano, G., Maggipinto, G., Tangaro, S., Castellano, M., et al. (2006). A completely automated CAD system for mass detection in a large mammographic database. *Medical Physics, 33*, 3066–3075.

Campanini, R., Dongiovanni, D., Iampieri, E., Lanconelli, N., Masotti, M., Palermo, G., et al. (2004). A novel featureless approach to mass detection in digital mammograms based on support vector machines. *Physics in Medicine and Biology, 49*, 961–975.

Chandrasekhar, R., & Attikiouzel, Y. (1997). A simple method for automatically locating the nipple on mammograms. *IEEE Transactions on Medical Imaging, 16*, 483–494.

Clausi, D. A. (2001). Comparison and fusion of co-occurrence, Gabor and MRF texture features for classification of SAR sea ice imagery. *Atmosphere-Ocean, 39*, 183–194.

Clausi, D. A. (2002). An analysis of co-occurrence texture statistics as a function of grey level quantization. *Canadian Journal of Remote Sensing, 28*, 45–62.

Davies, D. H., & Dance, D. R. (1990). Automatic computer detection of clustered calcifications in digital mammograms. *Physics in Medicine and Biology, 35*, 1111–1118.

Dheeba, J., Albert Singh, N., & Tamil Selvi, S. (2014). Computer-aided detection of breast cancer on mammograms: A swarm intelligence optimized wavelet neural network approach. *Journal of Biomedical Informatics, 49*, 45–52.

Eddaoudi, F., Regrgui, F., Mahmoudi, A., & Lamouri, N. (2011). Mass detection using SVM classifier based on texture analysis. *Applied Mathematical Science, 5*, 367–379.

Ferrari, R., & Rangayyan, R. (2004). Automatic identification of the pectoral muscle in Mammograms. *IEEE Transactions on Medical Imaging, 23*, 232–245.

Gonzalez, R. C., & Woods, R. E. (2008). *Digital image processing* (3rd ed.). N. J., Prentice Hall: Upper Saddle River.

Gray, A. (1997). *The intuitive idea of distance on a surface, §15.1 in modern differential geometry of curves and surfaces with mathematica* (2nd ed.). Boca Raton, FL: CRC Press, pp. 341-345.

Heath, M., Bowyer, K., Kopans, D., Kegelmeyer, W. P., Moore, R., & Chang, K. (1998). Current status of the digital database for screening mammography. In *Digital mammograpy* (pp. 457–460). Boston, MA, USA: Kluwer Academic Publishers. Available from: http://marathon.csee.usf.edu.

Karssemeijer, N. (1993). Adaptive noise equalization and recognition of microcalcification clusters in mammograms. *International Journal of Pattern Recognition and Artificial, 7*, 1357–1376.

Kwok, S., Chandrasekhar, R., & Attikiouzel, Y. (2001). Automatic pectoral muscle segmentation on mammograms by straight line estimation and cliff detection. In: *IIS conference* (pp. 67–72).

Lau, T. K., & Bischof, W. F. (1991). Automated detection of breast tumors using the asymmetry approach. *Computers and Biomedical Research, 24*, 273–295.

Liu, C. C., Tsai, C. Y., Tsui, T. S., & Yu, S. S. (2012). An improved GVF snake based breast region extrapolation scheme for digital mammograms. *Expert Systems with Applications, 39*, 4505–4510.

Maitra, I. K., Nag, S., & Bandyopadhyay, S. K. (2011). Technique for preprocessing of digital mammogram. *Computer Methods and Programs in Biomedicine, 107*, 175–188.

Martins, L. O., Junior, G. B., Silva, A. C., Paiva, A. C., & Gattass, M. (2009). Detection of masses in digital mammograms using K-means and support vector machine. *Electronics Letters on Computer Vision and Image Analysis, 8*, 39–50.

Meenalosini, S., & Janet, J. (2012). Computer aided diagnosis of malignancy in mammograms. *European Journal of Scientific Research, 72*, 360–368.

Mohamed, W. A., & Kadah, Y. M. (2007). Computer aided diagnosis of digital mammograms. *International Conference on Computer Engineering & Systems*, 299–303.

Mohd Khuzi, A., Besar, R., Wan Zaki, W. M. D., & Ahmad, N. N. (2009). Identification of masses in digital mammogram using gray level co-occurrence matrices. *Biomedical Imaging and Intervention Journal, 5*, e17.

Mudigonda, N. R., Rangayyan, R. M., & Desautels, J. E. (2000). Gradient and texture analysis for the classification of mammographic masses. *IEEE Transactions on Medical Imaging, 19*, 1032–1043.

Mustra, M., & Grgic, M. (2013). Robust automatic breast and pectoral muscle segmentation from scanned mammograms. *Signal Process, 93*, 2817–2827.

Nishikawa, R. M., & Yaffe, M. J. (1985). Signal-to-noise properties of mammographic film-screen systems. *Medical Physics, 12*, 32–39.

Ojala, T., Nappi, J., & Nevalainen, O. (2001). Accurate segmentation of the breast region from digitized mammograms. *Computerized Medical Imaging and Graphics, 25*, 47–59.

Otsu, N. (1979). A threshold selection method from gray-level histograms. *IEEE Transactions on Systems, Man, and Cybernetics, 9*(1), 62–66.

Pearson, K. (1901). Principal Components Analysis. The London, Edinburgh and Dublin Philosophical Magazine and Journal, 6 (pp. 566).

Roberto, R. P., Paulo, M. A. M., Marcelo, O. H., Sergio, K. K., Roger, E., Chisako, M., et al. (2006). Usefulness of texture analysis for computerized classification of breast lesion on mammograms. *Journal of Digital Imaging, 20*, 248–255.

Rojas, A., & Nandi, A. K. (2009). Toward breast cancer diagnosis based on automated segmentation of masses in mammograms. *Pattern Recognition, 42*, 1138–1148.

Sakai, N., Yonekawa, S., & Matsuzaki, A. (1996). Two dimensional image analysis of the shape of rice and its application to separating varieties. *Journal of Food Engineering, 27*, 397–407.

Sameti, M., Ward, R. K., Palcic, B., & Morgan-Parkes, J. (1997). Texture feature extraction for tumor detection in mammographic images. In: *Pacific rim conference on communications, computers and signal processing* (vol. 2, pp. 831–834).

Serra, J. (1982). *Image analysis and mathematical morphology*. London: Academic Press.

Shi, Y. Q., & Sun, H. (2008). *Image and video compression for multimedia engineering. fundamentals, algorithms, standards* (2nd ed.). CRC Press-Taylor & Francis Group.

Shokr, M. E. (1991). Evaluation of second-order texture parameters for sea ice classification from radar images. *Journal of Geophysical Research, 96*, 10625–10640.

Siddiqui, M. K., Anand, M., Mehrotr, P. K., Sarangi, R., & Mathur, N. (2005). Biomonitoring of organochlorines in women with benign and malignant breast disease. *Environmental Research, 98*, 250–257.

Suckling, J., Parker, J., Dance, D., Astley, S., Hutt, I., Boggis, C., et al. (1994). The mammographic image analysis society digital mammogram database. *Exerpta Medica, International Congress Series, 1069*, 375–378.

Swank, R. K. (1973). Absorption and noise in X-ray phosphors. *Journal of Applied Physics, 44*, 4199–4203.

Yonekawa, S., Sakai, N., & Kitani, O. (1996). Identification of idealized leaf types using simple dimensionless shape features by image analysis. *Transactions of the ASAE, 39*, 1525–1533.

Yuan, Y., Giger, M. L., Li, H., & Sennett, C. (2008). Correlative feature analysis of FFDM images. In: M.L. Giger, N. Karssemeijer (Eds.), Proceedings of SPIE medical imaging 2008, computer-aided diagnosis 6915.